# Interference of nuclear wave packets carrying different angular momenta in the dissociation of $H_2^+$ in strong circularly polarized laser pulses

Zhen Chen[1] and Feng He[1,2,*]

[1]*Key Laboratory for Laser Plasmas (Ministry of Education) and School of Physics and Astronomy, Collaborative Innovation Center of IFSA (CICIFSA), Shanghai Jiao Tong University, Shanghai 200240, China*

[2]*CAS Center for Excellence in Ultra-intense Laser Science, Shanghai 201800, China*

(Received 12 March 2020; accepted 25 August 2020; published 14 September 2020)

We systematically investigate the interference of nuclear wave packets carrying different angular momenta by numerically solving the time-dependent Schrödinger equation for the dissociation of $H_2^+$ in strong circularly polarized laser pulses. $H_2^+$ exposed to strong laser pulses may absorb different numbers of photons and dissociate along different pathways carrying different angular momenta. In case dissociation pathways differ by an even number of photons, the respective wave packets have the same parity and thus interfere with each other, leading to spiral nuclear momentum distributions for the dissociative fragments. Inversely, by investigating the interference structure of the angle-resolved kinetic energy release of the dissociative fragments, the molecular dissociation pathways can be extracted. The spiral nuclear momentum distribution provides another approach to explore ultrafast molecular dynamics.

DOI: 10.1103/PhysRevA.102.033107

## I. INTRODUCTION

When exposed to strong laser fields, molecules may absorb photons and thus chemical reactions occur [1]. In one case, the electron takes enough photon energy and becomes free, which is termed as photoionization and has been extensively studied. In another case, the electron may not take enough energy to be freed, but jump to excited electronic states followed by the molecular bond breaking. This scenario is termed as molecular dissociation. As the simplest molecules in nature, $H_2^+$ and its isotopes have worked as the model to understand the molecular dissociation for decades [2–4]. In this paper, we focus on the dissociation of $H_2^+$ in circularly polarized laser fields.

When investigating the dissociation of $H_2^+$, the Born-Oppenheimer approximation [5] is widely adopted, which means the molecular wave function can be written as the product of the electronic part and the nuclear part. Specifically, the wave function of $H_2^+$ can be expressed as $\psi = \sum_j \chi_j(\mathbf{R}, t)\varphi_j(\mathbf{r}, \mathbf{R})$, where $\chi_j(\mathbf{R}, t)$ is the nuclear wave function and $\varphi_j(\mathbf{r}, \mathbf{R})$ is the R-parametric electron wave function. $\mathbf{R}$ and $\mathbf{r}$ are the internuclear distance and electron coordinate, respectively, and $j$ is the index of the electronic state. In most cases the physical dynamics of $H_2^+$ dissociation are dominated by two lowest electronic states, namely $1s\sigma_g$ and $2p\sigma_u$, which makes the theoretical analysis transparent [6,7].

In past decades, a series of dissociation pathways of $H_2^+$ in strong laser fields have been explored. Due to the opposite parity between $1s\sigma_g$ and $2p\sigma_u$ states, $H_2^+$ in the $1s\sigma_g$ state can only absorb an odd number of photons and jump to the repulsive $2p\sigma_u$ state. The corresponding dissociation pathways are termed as the one-photon pathway [8,9], three-photon pathway [10,11], and so on. The wave packet of three-photon pathway on the $2p\sigma_u$ state may emit one photon and jump back to the $1s\sigma_g$ state, in which case the net-two-photon pathway [12] dominates the dissociation process. Besides the pathways mentioned above, the excitation of $H_2^+$ can be mediated by the electron-electron correlation. Specifically, the ionized electron of $H_2$ may be driven back to the remaining $H_2^+$ by the laser field and share its energy with the bound electron via the rescattering process [13,14]. It is generally accepted that different dissociation pathways can be identified by analyzing the kinetic energy release (KER) of dissociative fragments [15]. However, due to the broad kinetic energy distribution of the nuclear vibrational states of $H_2^+$ [16], different dissociation pathways may end with similar KER, which makes it difficult to resolve them. The interference of different pathways with opposite parity leads to the asymmetric electron localization on two nuclei [13,17]. For example, when $H_2^+$ undergoes one- and net-two-photon pathways, the electron oscillates between two nuclei. The electron hopping stops when the interatomic barrier is high enough to prohibit the electronic movement between two nuclei [18,19]. The preference of localization direction fundamentally depends on the phase difference of coexistent dissociation pathways. The electron localization can be controlled by tuning the relative phase of dissociation pathways between $1s\sigma_g$ and $2p\sigma_u$ states with numerous strategies [13,17–33].

Although there are lots of studies focusing on the nuclear energy, few investigations pay attention to the angular momenta of dissociative fragments. Recently, we studied the dissociation of $H_2^+$ in a circularly polarized laser pulse, and found that the coexistent one- and three-photon pathways

*fhe@sjtu.edu.cn

 

interfere with each other, resulting in the spiral nuclear momentum distribution [34]. In this paper, we systematically study the interference of different dissociation pathways in molecular dissociation. Under the irradiation of one or two strong circularly polarized laser pulses, $H_2^+$ may dissociate by absorbing net-zero photon, one photon, net-two photons, three photons, five, or even seven photons. Dissociation pathways with the same parity may interfere with each other and thus produce abundant angle-resolved dissociation scenarios. The paper is organized as follows. In Sec. II we briefly introduce the theoretical method used in our calculations. Main results and discussions are presented in Sec. III. Finally, a summary is given in Sec. IV. Atomic units are used throughout the paper unless otherwise stated.

## II. NUMERICAL METHODS

Since the dissociation of $H_2^+$ is mainly governed by the two lowest electronic states, we therefore numerically solve the two-channel time-dependent Schrödinger equation [32,35]

$$i\frac{\partial}{\partial t}\begin{pmatrix}\chi_g(R_x,R_y,t)\\ \chi_u(R_x,R_y,t)\end{pmatrix}=\begin{pmatrix}\frac{P_x^2+P_y^2}{2M}+V_g(R_x,R_y) & D(R_x,R_y)F(t)\\ D(R_x,R_y)F(t) & \frac{P_x^2+P_y^2}{2M}+V_u(R_x,R_y)\end{pmatrix}\begin{pmatrix}\chi_g(R_x,R_y,t)\\ \chi_u(R_x,R_y,t)\end{pmatrix}, \tag{1}$$

where $\chi_g(R_x,R_y,t)$ and $\chi_u(R_x,R_y,t)$ are the nuclear wave packets associated with the electronic states $1s\sigma_g$ and $2p\sigma_u$, respectively. Considering that along the laser propagation direction there are no important physical dynamics except for some trivial nuclear wave packet expansion, we concentrate on the nuclear movements in the laser polarization plane. $M=918$ a.u. is the reduced nuclear mass, $P_x$ and $P_y$ are the nuclear momentum operators, and $V_g(R_x,R_y)$, $V_u(R_x,R_y)$ are the potential surfaces for the $1s\sigma_g$ and $2p\sigma_u$ states, respectively. $D(R_x,R_y)$ is the transition dipole moment representing the coupling action between the two electronic states. $F(t)$ is the laser electric field to be used. In our simulations, the ground nuclear state of $H_2$ is used as the initial state $\chi_g(R_x,R_y,t=0)$ according to the Franck-Condon approximation, and we set $\chi_u(R_x,R_y,t=0)=0$. Physically, such an initial state may be produced by ionizing $H_2$ with a circularly polarized attosecond pulse [36,37]. Numerically, such an initial state can be obtained by searching for the ground nuclear rovibrational state of $H_2$ using the imaginary-time propagation method [38]. After freely propagating the initial nuclear wave packet on the $1s\sigma_g$ potential surface for time $t_0$, we introduce the laser field

$$\mathbf{F}(t)=\mathbf{F}_1(t-t_0)+\mathbf{F}_2(t-t_0-\Delta t) \tag{2}$$

with

$$\mathbf{F}_1(t)=E_1[\cos(\omega_1 t+\alpha_1)\hat{x}+\sin(\omega_1 t+\alpha_1)\hat{y}]\times\sin^2(\pi t/L_1),\ t_0<t<t_0+L_1 \tag{3}$$

and

$$\mathbf{F}_2(t)=E_2[\cos(\omega_2 t+\alpha_2)\hat{x}-\sin(\omega_2 t+\alpha_2)\hat{y}]\times\sin^2(\pi t/L_2),\ t_0+\Delta t<t<t_0+\Delta t+L_2 \tag{4}$$

to dissociate $H_2^+$. $\mathbf{F}_1(t)$ and $\mathbf{F}_2(t)$ are left- and right-circularly polarized, respectively. $E_1$ and $E_2$, $\omega_1$ and $\omega_2$, $\alpha_1$ and $\alpha_2$, $L_1$ and $L_2$ are the field amplitude, angular frequency, carrier-envelope phase (CEP), and pulse duration of the two pulses, respectively. We set $t_0=5$ fs and $\alpha_1=\alpha_2=0$ throughout the simulations. $\Delta t$ is the time delay of the two pulses. The split-operator algorithm is used to propagate the wave packet in the laser field [39]. The spatial steps in simulations are $dR_x=dR_y=0.02$ a.u., and the time step is $dt=0.2$ a.u.. The simulation box is big enough ($-100$ a.u. $\leqslant R_{x/y}\leqslant 100$ a.u.) to avoid the nuclear wave packet hitting the boundary. The convergence of the simulations has been verified. After the laser field is over, we keep propagating the nuclear wave packet until the dissociative parts have separated from the bound vibration states. By Fourier transforming the dissociative wave packets $\chi_{g/u}(R_x,R_y)$ (in the area $R>10$ a.u.) of $1s\sigma_g$ and $2p\sigma_u$ states, we obtain the nuclear wave packets in momentum representation

$$\tilde{\chi}_{g/u}(P_x,P_y)=\iint dR_x dR_y \chi_{g/u}(R_x,R_y)\times\exp[-i(P_xR_x+P_yR_y)]. \tag{5}$$

The nuclear momentum distribution is thus expressed as [40]

$$W(P_x,P_y)=|\tilde{\chi}_g(P_x,P_y)|^2+|\tilde{\chi}_u(P_x,P_y)|^2. \tag{6}$$

The angle-resolved KER distribution can be obtained by tossing the probability at $(P_x,P_y)$ into the bin at $(\phi,K)$, where $\phi=\arctan(P_y/P_x)$ is the nuclear emission angle and $K=(P_x^2+P_y^2)/2M$ is the KER.

## III. RESULTS AND DISCUSSIONS

First, we consider the dissociation of $H_2^+$ in a single infrared (IR) laser pulse. In calculations, we set $\mathbf{F}_2=0$ in Eq. (2). Figures 1(a), 1(b) show the nuclear momentum distributions and Figs. 1(c), 1(d) show the corresponding angle-resolved KER distributions. All the figures in this paper are logarithmic with the base of 10. 800 nm and 1600 nm laser pulses are used in the left and right columns, respectively. In both columns, the laser pulse has the peak intensity $10^{14}$ W/cm$^2$ (corresponding to $E_1=0.0377$ a.u.) and pulse duration four optical cycles. Archimedes spiral structures appear in the momentum distributions. We parenthetically point out that similar interference structures have been numerically predicted and experimentally observed in photoelectron momentum distributions [41–45].

The spiral nuclear momentum distribution can be well understood in the angle-resolved KER representation. Once $H_2^+$ absorbs $m_j$ photons from the laser pulse, the molecular wave packet of this pathway carries the angular momentum $m_j\hbar$. For two coexistent dissociation pathways both from either $1s\sigma_g$ or $2p\sigma_u$ state, the superimposed wave packet can be

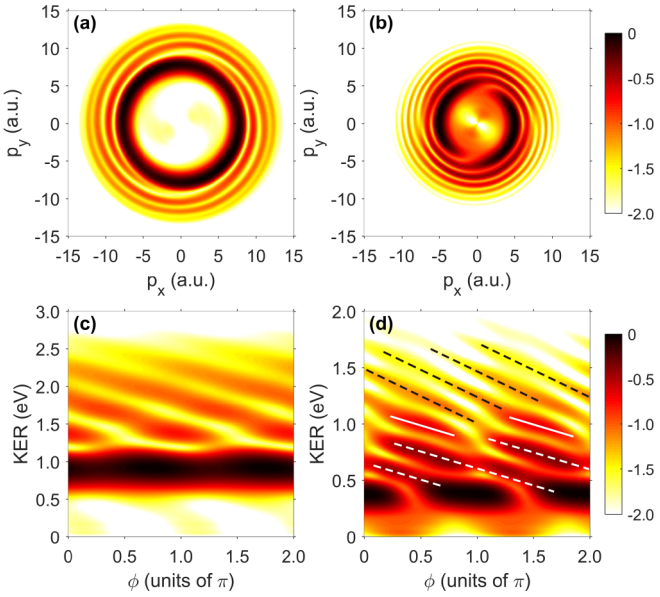


FIG. 1. (a), (b) The dissociative nuclear momentum distributions. (c), (d) The angle-resolved KER distributions corresponding to (a) and (b), respectively. Laser pulses with the wavelengths 800 nm and 1600 nm are used in (a), (c) and (b), (d), respectively. The laser intensity and duration of both pulses are $10^{14}$ W/cm$^2$ and four optical cycles.

expressed as

$$\tilde{\chi}_{g/u}(\phi, K) = \sum_{j=1,2} A_j(K) e^{i[m_j(\phi+\alpha_j)+\eta_j(K)]}, \tag{7}$$

where $A_j(K)$ is the amplitude for the $j$th pathway and $\eta_j(K)$ is a KER-dependent phase term. The interference structure contributed by these two dissociation pathways could thus arise in the angle-resolved KER distribution according to

$$\begin{aligned} |\tilde{\chi}_{g/u}(\phi, K)|^2 = {} & A_1^2(K) + A_2^2(K) + 2A_1(K)A_2(K) \\ & \times \cos\{\Delta m[\phi + (m_2\alpha_2 - m_1\alpha_1)/\Delta m] \\ & + \Delta\eta(K)\} \end{aligned} \tag{8}$$

with $\Delta m = m_2 - m_1$ and $\Delta\eta(K) = \eta_2(K) - \eta_1(K)$. The cross term in Eq. (8) produces the interference pattern oscillating as $\phi$ with the period $2\pi/\Delta m$. The constant phase term $(m_2\alpha_2 - m_1\alpha_1)/\Delta m$ indicates that, variation of the CEP of the two laser pulses will induce the rotation of spiral momentum distribution and horizontal translation of angle-resolved KER distribution [42,43]. This constant phase term equals $\alpha_1$ in the single-color field case in Fig. 1.

As reported in Ref. [34], the spiral nuclear momentum distribution shown in Fig. 1(a) is due to the interference of one- and three-photon dissociation pathways carrying the angular momentum $\hbar$ and $3\hbar$, respectively. Consequently, for a given KER the dissociation probability oscillates as $\phi$ with the period $\pi$ for the range KER $\in$ [1.2 eV 3 eV] in Fig. 1(c). The dissociative fragments with the KER below 1.2 eV in Fig. 1(c) is purely contributed by the one-photon dissociation pathway.

The momentum distribution shown in Fig. 1(b) for the 1600 nm case also presents the Archimedes spiral structure. More complex structures can be found in the angle-resolved KER in Fig. 1(d). We have confirmed that almost all dissociative fragments still dissociate along the $2p\sigma_u$ state, and thus the dissociation could be one-, three-, and five-photon pathways. In Fig. 1(d), the angle-dependent KER distribution can be roughly divided into two parts below and above the energy 1.1 eV, respectively. For the part above the energy 1.1 eV, the interference pattern guided by the black dashed lines varies as $\phi$ with the period $\pi/2$, indicating four-photon difference of the two interference pathways according to Eq. (8). One may conclude that this part is induced by the interference of one- and five-photon dissociation pathways. The stripes below 1.1 eV guided by the white solid lines and white dashed lines vary as $\phi$ with the period $\pi$, indicating that they are produced by the interference of pathways differing by two photons. Two possible interference paths contribute to them, i.e., the interference of three- and five-photon pathways or the interference of three- and one-photon pathways.

The interference structures along the KER direction in Figs. 1(c) and 1(d) are induced by the phase difference $\Delta\eta(K)$. $\Delta\eta(K)$ contains the time information about the molecule relaxing to a certain internuclear distance. By extracting the phase term $\Delta\eta(K)$ from the interference stripes in Figs. 1(c) and 1(d), one can evaluate the time difference between one- and three-photon or five-photon pathways.

Above we have shown the spiral interference patterns created by the superposition of nuclear wave packets from different dissociation pathways initiated by the same one pulse. In the sections that follow, by using two-color laser pulses we investigate the interference of nuclear wave packets released by two pulses sequentially. First we use two counterrotating circularly polarized extreme ultraviolet (XUV) pulses to dissociate $H_2^+$. The left and right columns of Fig. 2 show the nuclear momentum and corresponding angle-dependent KER distributions, respectively. In Figs. 2(a) and 2(b), the used laser parameters are $E_1 = E_2 = 0.0377$ a.u. (i.e., peak intensity $I_1 = I_2 = 10^{14}$ W/cm$^2$), $\omega_1 = \omega_2 = 0.4$ a.u. (i.e., wavelength $\lambda_1 = \lambda_2 = 114$ nm), $L_1 = L_2 = 1.52$ fs (four optical cycles) and $\Delta t = 2.28$ fs (six optical cycles). The used photon energy $\omega_1 = \omega_2 = 0.4$ a.u. is close to the resonance-transition energy gap (0.43 a.u.) between the potential curves of $1s\sigma_g$ and $2p\sigma_u$ states at the equilibrium internuclear distance of the $1s\sigma_g$ state ($R = 2$ a.u.). One-photon pathway dominates the dissociation process and the KER is centered at around 7.0 eV. The two counterrotating pulses excite two dissociative nuclear wave packets carrying angular momenta $\hbar$ and $-\hbar$ respectively, whose interference results in two spiral arms in the nuclear momentum vortex in Fig. 2(a). As expected, the corresponding angle-resolved KER shown in Fig. 2(b) presents the interference stripes varying as $\phi$ with the period $\pi$.

In Figs. 2(c) and 2(d), the used laser parameters are $E_1 = E_2 = 0.0377$ a.u. ($I_1 = I_2 = 10^{14}$ W/cm$^2$), $\omega_1 = \omega_2 = 0.13$ a.u. ($\lambda_1 = \lambda_2 = 342$ nm), $L_1 = L_2 = 4.56$ fs (four optical cycles) and $\Delta t = 6.84$ fs (six optical cycles). Three distinct interference signals are observed. In the range KER $\in$ [1 eV, 3 eV] in Fig. 2(d), the fragments dissociate along the $2p\sigma_u$ state and the interference stripes show the $\pi$-periodical variation as $\phi$. Similar to Fig. 2(b), this interference is contributed by two dissociating wave packets absorbing one photon with the left and right helicity, respectively. By

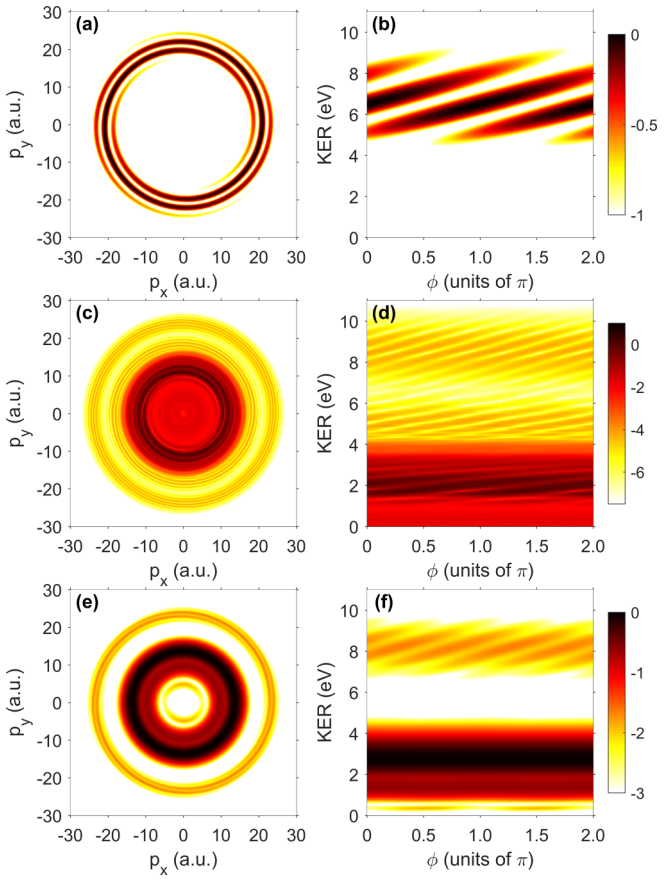


FIG. 2. (a), (c), (e) The nuclear momentum distributions and (b), (d), (f) the corresponding angle-resolved KER distributions. In each row, two counterrotating pulses are used for dissociation. (a), (b) The wavelength, intensity and duration of the both pulses are 114 nm, $10^{14}$ W/cm$^2$ and 1.52 fs. (c), (d) The wavelength, intensity and duration of the both pulses are 342 nm, $10^{14}$ W/cm$^2$ and 4.56 fs. (e), (f) The wavelengths, intensities and durations of the first and second pulses are 114 nm and 342 nm, $10^{11}$ W/cm$^2$ and $10^{14}$ W/cm$^2$, 1.52 fs and 4.56 fs, respectively.

tracing the time-dependent molecular wave packets we know the fragments with KER $\in$ [4 eV, 6 eV] dissociate along the $1s\sigma_g$ state, indicating that the net-two-photon pathway dominates the dissociation process in this energy range. Consequently, the KER varies as $\phi$ with the period $\pi/2$. The fragments with energy higher than 7 eV are contributed by the three-photon dissociation. Therefore, the interference of two wave packets carrying angular momenta $3\hbar$ and $-3\hbar$ gives rise to the angle-resolved KER with the period $\pi/3$ in the $\phi$ direction.

In Figs. 2(e) and 2(f), we use the laser parameters $E_1 = 0.0012$ a.u. and $E_2 = 0.0377$ a.u. ($I_1 = 10^{11}$ W/cm$^2$ and $I_2 = 10^{14}$ W/cm$^2$), $\omega_1 = 0.4$ a.u. and $\omega_2 = 0.13$ a.u. ($\lambda_1 = 114$ nm and $\lambda_2 = 342$ nm), $L_1 = 1.52$ fs and $L_2 = 4.56$ fs (four optical cycles) and $\Delta t = 6.84$ fs (six optical cycles for 342 nm). Note that the three-photon pathway of 342 nm and the one-photon pathway of 114 nm give almost the same KER. In the range KER $\in$ [7 eV, 9 eV] in Fig. 2(f) clear interference patterns induced by these two pathways are observed. Since the two pulses have opposite helicity, the interference with the period

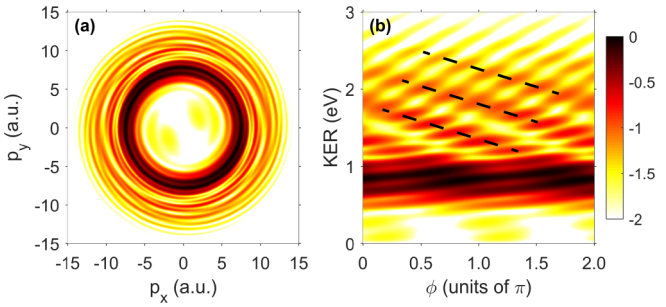


FIG. 3. (a) The dissociative nuclear momentum distribution and (b) the angle-resolved KER distribution initiated by two counterrotating 800 nm laser pulses. Both pulses have the intensity $10^{14}$ W/cm$^2$ and the duration 10.67 fs. The time delay between two pulses is 16 fs.

$\pi/2$ is present. To achieve clear interference fringes, the intensity of 114 nm is three orders of magnitude weaker than that of the 342 nm pulse. The key to observing clear interference vortex of two dissociation pathways is that they have overlap in KER and comparable probabilities. The signal presenting as a horizontal band in the range KER <4 eV comes from the one-photon channel of 342 nm.

In Fig. 3 we examine the interference structure when two time-delayed counterrotating IR pulses are used to dissociate $H_2^+$. Figures 3(a) and 3(b) show the corresponding nuclear momentum and KER distributions. The applied laser parameters are $E_1 = E_2 = 0.0377$ a.u. ($I_1 = I_2 = 10^{14}$ W/cm$^2$), $\omega_1 = \omega_2 = 0.057$ a.u. ($\lambda_1 = \lambda_2 = 800$ nm), $L_1 = L_2 = 10.67$ fs (four optical cycles), and $\Delta t = 16$ fs (six optical cycles). The dissociation along the $2p\sigma_u$ state contributes to almost all the signals here. One may expect that the interference of one- and three-photon pathways initiated by the same one pulse, and the interference of two pathways initiated by two pulses sequentially, may arise together, which is indeed the case as shown in Fig. 3(b). Overall, one can see two sets of interference fringes, i.e., one with positive slope and the other with negative slope. According to the discussions about Fig. 1(c), one is informed that the stripes with negative slope (as guided by the black dashed lines) are contributed by the interference of one- and three-photon dissociation pathways initiated by the same one pulse. The stripes with positive slopes, which can be divided into two parts, are due to the interference of two wave packets initiated by two pulses sequentially. For the part with energy below 1 eV, the stripes with positive slope and large probability are contributed by the interference of two nuclear wave packets carrying angular momentum $\hbar$ and $-\hbar$ by absorbing one photon with left and right helicity from two pulses, respectively. For the part with energy above 1.5 eV the stripes with positive slope show the period $\pi/3$ as $\phi$, indicating that this interference is induced by two three-photon pathways by absorbing three photons from two pulses, respectively. The superposition of two sets of interference fringes with positive and negative slopes gives rise to the gridlike pattern in the range KER $\in$ [1.5 eV, 3 eV].

In above discussions, the nuclear wave packets along the $2p\sigma_u$ state dominate the dissociation, and the fragments from the $1s\sigma_g$ state have low probabilities. However, by constructing the two-color laser field with proper pulse parameters,

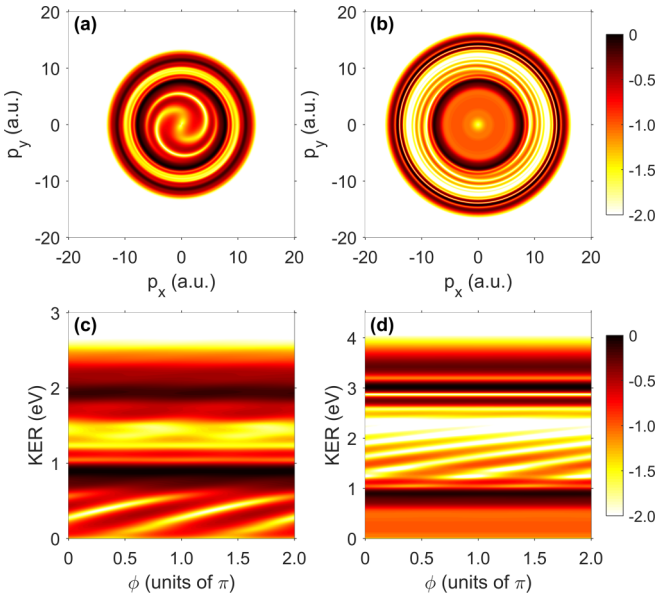


FIG. 4. (a), (b) The dissociative nuclear momentum distributions and (c), (d) the corresponding angle-resolved KER distributions. (a), (c) Counterrotating 800 nm and 400 nm laser fields are used. Both the pulses have the intensity $10^{12}$ W/cm$^2$ and duration 27.67 fs. The time delay of them is 0. (b), (d) Counterrotating 800 nm and 266 nm laser fields are used, and other laser parameters are the same as those in (a), (c).

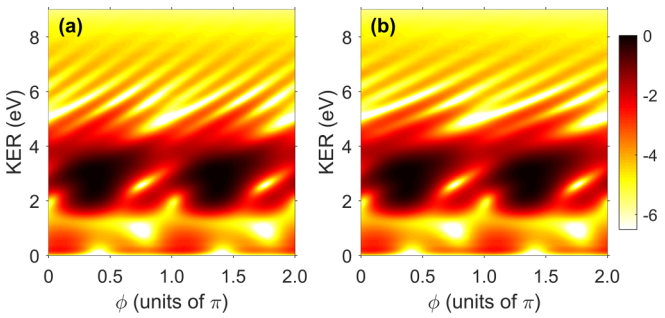


FIG. 5. The angle-resolved KER distributions when (a) counterrotating and (b) corotating two-color pulses are used. In (a) and (b), $\lambda_1 = 800$ nm and $\lambda_2 = 114$ nm, $I_1 = 2 \times 10^{14}$ W/cm$^2$ and $I_2 = 10^{10}$ W/cm$^2$, $L_1 = 10.67$ fs and $L_2 = 1.52$ fs. The time delay between the two pulses is 16 fs.

the dissociation along the $1s\sigma_g$ state such as zero-photon and net-two-photon pathways may have non-negligible contributions. Here we dissociate $H_2^+$ with the 800 nm laser pulse plus its harmonics. The nuclear momentum distributions are shown in Figs. 4(a), 4(b) and the angle-resolved KERs are shown in Figs. 4(c), 4(d). In the left column, the used laser parameters are $E_1 = E_2 = 0.0038$ a.u. ($I_1 = I_2 = 10^{12}$ W/cm$^2$), $\omega_1 = 0.057$ a.u. and $\omega_2 = 0.114$ a.u. ($\lambda_1 = 800$ nm and $\lambda_2 = 400$ nm), $L_1 = L_2 = 26.67$ fs (ten optical cycles of 800 nm), and $\Delta t = 0$. In the right column, the 400 nm pulse is replaced by a 266 nm pulse and other parameters are kept unchanged. Two counterrotating pulses are applied here. The three parts showing horizontal bands around KER $\approx$0.9 eV, 2 eV, and 3 eV in Figs. 4(c) and 4(d) are solely contributed by the one-photon pathway of 800 nm, 400 nm, and 266 nm pulse, respectively. Next we focus on the parts with interference structures.

With the two-state numerical model we are able to identify that the stripes with the energy less than 0.8 eV in Fig. 4(c) are all from the $1s\sigma_g$ state. This part varies as $\phi$ with the period $\pi$, indicating that the interference is contributed by two pathways differing by two photons. Considering the relatively weak laser used in this calculation, we thus conclude that the interference is induced by the following two pathways. One is the direct pathway, also known as the zero-photon process in which some high-energy wave packet of the initial state can directly dissociate along the $1s\sigma_g$ state without absorbing any photon, and the angular momentum of this part is 0. The other pathway is the net-zero pathway [46], for which $H_2^+$ first absorbs a left-circularly polarized 400 nm photon and emits a right-circularly polarized 800 nm photon later, ending with dissociation also along the $1s\sigma_g$ state with very low KER. The nuclear wave packet dissociating through such a net-zero-photon pathway carries the angular momentum $2\hbar$ since the 800 nm and 400 nm photons have opposite helicity. In Fig. 4(d) similar interference structure can be seen in the range KER $\in$ [1 eV, 2 eV], and the physical mechanism behind it is the same as that described in Fig. 4(c). By the way, we point out that the angular momentum of the dissociative wave packet given by the net-zero-photon pathway is 0 if two corotating pulses are used. In that case one would expect that no $\phi$-dependent interference structures appear. Our numerical tests have proved that it is indeed the case.

Though one-, net-two-, and three-photon dissociation pathways have been studied extensively, the high-order above-threshold dissociations (HATD), i.e., pathways involving four or more photons have been discussed in only a few studies [14,47,48]. It was not until 2018 that the work [14] reported the unambiguous experimental observation of the HATD pathway of $H_2$ in strong laser fields. In this section, we pursue a theoretical route to observe the HATD pathway by taking advantage of the interference of different dissociation pathways discussed above. In most of the current research the HATD process of $H_2$ is mediated by the electron-electron correlation. Here we identify the direct HATD pathway in a simpler system, i.e., $H_2^+$, where the electron-electron correlation is not present.

The results are shown in Fig. 5. Here $H_2^+$ is dissociated by the XUV + IR two-color field. The laser parameters are $E_1 = 0.0534$ a.u. and $E_2 = 0.0004$ a.u. ($I_1 = 2 \times 10^{14}$ W/cm$^2$ and $I_2 = 10^{10}$ W/cm$^2$), $\omega_1 = 0.057$ a.u. and $\omega_2 = 0.400$ a.u. ($\lambda_1 = 800$ nm and $\lambda_2 = 114$ nm), $L_1 = 10.67$ fs and $L_2 = 1.52$ fs (four optical cycles) and $\Delta t = 16$ fs (six optical cycles of 800 nm). In Fig. 5(a), the 800 nm pulse and 114 nm pulse are left- and right-circularly polarized, respectively. In Fig. 5(b), both pulses are left-circularly polarized. The 114 nm pulse can only initiate the one-photon pathway because its photon energy is so large that other high-order dissociation processes can be ignored. The 800 nm pulse can possibly bring about the high-order, such as five- or seven-photon dissociation pathways. Our simulation results show that ignoring the ionization process here in our numerical model is reasonable. Once $H_2^+$ directly absorbs multiple

800 nm photons or a single 114 nm photon, the wave packets propagate along the $2p\sigma_u$ state and interference may occur if the two pathways end with the overlapped KER. According to the analysis above, one can identify how many 800 nm photons are absorbed by counting the interference stripes in the angle-resolved KER distribution. The peak intensity of the 114 nm is smaller than that of 800 nm here to make the probabilities of these two pathways comparable to form clear interference fringes. The expected interference does appear in Fig. 5. Both of the 114 nm pulse and 800 nm pulse excite the nuclear wave packets with broad KER distributions, and they interfere in the range KER $\in$ [4 eV, 8 eV]. The interference fringes in Figs. 5(a) and 5(b) can be separated into two parts, which are brought about by two different interference mechanisms. For the higher-energy region KER $\in$ [6 eV, 8 eV] in Fig. 5(a), the interference stripes vary as $\phi$ with the period $\pi/4$. It is generated by the interference of one 114 nm photon pathway carrying the angular momentum $-\hbar$ and seven 800 nm photon pathway carrying the angular momentum $7\hbar$. While for the lower-energy region KER $\in$ [4 eV, 6 eV] six interference stripes are present, which indicates the interference of one 114 nm photon pathway and five 800 nm photon pathway. Similarly, in Fig. 5(b) when two pulses are corotating, the interference of one 114 nm photon channel with the angular momentum $\hbar$ and seven 800 nm photon channel with the angular momentum $7\hbar$ brings six stripes and $\pi/3$ interference period in the range KER $\in$ [6 eV, 8 eV] when $\phi$ changes from 0 to $2\pi$. While for the range KER $\in$ [4 eV, 6 eV], the interference fringes have four stripes, which are given by the interference of one 114 nm photon channel with the angular momentum $\hbar$ and five 800 nm photon channel with the angular momentum $5\hbar$. The inhomogeneity of the interference structures in the range KER $\in$ [4 eV, 6 eV] is possibly due to some minor contamination, such as the interference of five- and seven-photon pathways both from the 800 nm pulse. In short, by investigating the interference structure in the angle-resolved KER distribution, we identify the direct five-photon and seven-photon dissociation pathways. In experiments the direct observation of five- or seven-photon pathway is difficult. It is because the five- or seven-photon absorption occurs near the equilibrium internuclear distance, where the initial nuclear wave packet has a broad kinetic energy distribution. Besides that, the nonresonant excitation may also shift the energy peaks. All these factors make it difficult to identify the HATD pathways merely by analyzing the KER distribution. Our method of looking into the angular momentum has the advantage over the conventional method.

The observed interference structures in nuclear wave packets given by our two-state model are reliable. Including more electronic states in the numerical model does not bring noticeable changes for the interference structures [12,32,49]. By changing the laser peak intensity for a wide range, it is verified that the presented interference structures are robust to the field intensity, and can survive the focal volume averaging effect [50]. With the CEP-stable few-cycle pulses they may be observed in future experiments.

## IV. SUMMARY

In conclusion, the angle-resolved dissociation of $H_2^+$ in circularly polarized laser fields is studied by solving the time-dependent Schrödinger equation. Archimedes spiral nuclear momentum distributions and interference stripes with different slopes in angle-resolved KER distributions are observed when one or two circularly polarized laser pulses are introduced. With the help of angular momentum analysis, we clarify that the observed structures are contributed by the interference of two dissociation pathways with the same parity. This interference is fundamentally different from the one well accepted in the explanation of electron localization, where the interference of two pathways with opposite parity is necessary. By counting the interference stripes the dissociation pathways can be identified, though different pathways may have overlapped KER and are thus not possible to be resolved by only the KER distribution. Some optical strategies can be designed to extract the temporal information of molecular dissociation and time the ultrafast molecular dynamics with the assistance of nuclear angular momentum.

## ACKNOWLEDGMENTS

This work is supported by National Key R&D Program of China (2018YFA0404802), Innovation Program of Shanghai Municipal Education Commission (2017-01-07-00-02-E00034), National Natural Science Foundation of China (NSFC) (Grants No. 11574205, No. 11721091, No. 91850203), and Shanghai Shuguang Project (17SG10). Simulations were performed on the $\pi$ supercomputer at Shanghai Jiao Tong University.

[1] M. Nisoli, P. Decleva, F. Calegari, A. Palacios, and F. Martín, Chem. Rev. **117**, 10760 (2017).
[2] A. Giusti-Suzor, F. H. Mies, L. F. DiMauro, E. Charron, and B. Yang, J. Phys. B **28**, 309 (1995).
[3] C. R. Calvert, W. A. Bryan, W. R. Newell, and I. D. Williams, Phys. Rep. **491**, 1 (2010).
[4] H. Ibrahim, C. Lefebvre, A. D. Bandrauk, A. Staudte, and F. Légaré, J. Phys. B **51**, 042002 (2018).
[5] B. H. Bransden and C. J. Joachain, *Physics of Atoms and Molecules* (Prentice Hall, New York, 2003).
[6] H. Niikura, P. B. Corkum, and D. M. Villeneuve, Phys. Rev. Lett. **90**, 203601 (2003).
[7] B. Feuerstein, Th. Ergler, A. Rudenko, K. Zrost, C. D. Schröter, R. Moshammer, J. Ullrich, T. Niederhausen, and U. Thumm, Phys. Rev. Lett. **99**, 153002 (2007).
[8] A. D. Bandrauk and M. L. Sink, J. Chem. Phys. **74**, 1110 (1981).
[9] P. H. Bucksbaum, A. Zavriyev, H. G. Muller, and D. W. Schumacher, Phys. Rev. Lett. **64**, 1883 (1990).
[10] A. Giusti-Suzor and F. H. Mies, Phys. Rev. Lett. **68**, 3869 (1992).

[11] J. McKenna, F. Anis, A. M. Sayler, B. Gaire, N. G. Johnson, E. Parke, K. D. Carnes, B. D. Esry, and I. Ben-Itzhak, Phys. Rev. A **85**, 023405 (2012).

[12] A. Staudte, D. Pavičić, S. Chelkowski, D. Zeidler, M. Meckel, H. Niikura, M. Schöffler, S. Schössler, B. Ulrich, P. P. Rajeev, T. Weber, T. Jahnke, D. M. Villeneuve, A. D. Bandrauk, C. L. Cocke, P. B. Corkum, and R. Dörner, Phys. Rev. Lett. **98**, 073003 (2007).

[13] M. F. Kling, C. Siedschlag, A. J. Verhoef, J. I. Khan, M. Schultze, T. Uphues, Y. Ni, M. Uiberacker, M. Drescher, F. Krausz, and M. J. J. Vrakking, Science **312**, 246 (2006).

[14] P. Lu, J. Wang, H. Li, K. Lin, X. Gong, Q. Song, Q. Ji, W. Zhang, J. Ma, H. Li, H. Zeng, F. He, and J. Wu, Proc. Natl. Acad. Sci. USA **115**, 2049 (2018).

[15] W. Zhang, X. Gong, H. Li, P. Lu, F. Sun, Q. Ji, K. Lin, J. Ma, H. Li, J. Qiang, F. He, and J. Wu, Nature Commu. **10**, 757 (2019).

[16] J. Wu, M. Kunitski, M. Pitzer, F. Trinter, L. Ph. H. Schmidt, T. Jahnke, M. Magrakvelidze, C. B. Madsen, L. B. Madsen, U. Thumm, and R. Dörner, Phys. Rev. Lett. **111**, 023002 (2013).

[17] D. Ray, F. He, S. De, W. Cao, H. Mashiko, P. Ranitovic, K. P. Singh, I. Znakovskaya, U. Thumm, G. G. Paulus, M. F. Kling, I. V. Litvinyuk, and C. L. Cocke, Phys. Rev. Lett. **103**, 223201 (2009).

[18] F. He, C. Ruiz, and A. Becker, Phys. Rev. Lett. **99**, 083002 (2007).

[19] F. He, A. Becker, and U. Thumm, Phys. Rev. Lett. **101**, 213002 (2008).

[20] V. Roudnev, B. D. Esry, and I. Ben-Itzhak, Phys. Rev. Lett. **93**, 163601 (2004).

[21] V. Roudnev and B. D. Esry, Phys. Rev. Lett. **99**, 220406 (2007).

[22] M. Kremer, B. Fischer, B. Feuerstein, V. L. B. de Jesus, V. Sharma, C. Hofrichter, A. Rudenko, U. Thumm, C. D. Schröter, R. Moshammer, and J. Ullrich, Phys. Rev. Lett. **103**, 213003 (2009).

[23] F. Kelkensberg, C. Lefebvre, W. Siu, O. Ghafur, T. T. Nguyen-Dang, O. Atabek, A. Keller, V. Serov, P. Johnsson, M. Swoboda, T. Remetter, A. L'Huillier, S. Zherebtsov, G. Sansone, E. Benedetti, F. Ferrari, M. Nisoli, F. Lépine, M. F. Kling, and M. J. J. Vrakking, Phys. Rev. Lett. **103**, 123005 (2009).

[24] G. Sansone, F. Kelkensberg, J. F. P. Torres, F. Morales, M. F. Kling, W. Siu, O. Ghafur, P. Johnsson, M. Swoboda, E. Benedetti, F. Ferrari, F. Lépine, J. L. S. Vicario, S. Zherebtsov, I. Znakovskaya, A. L'Huillier, M. Y. Ivanov, M. Nisoli, F. Martín, and M. J. J. Vrakking, Nature (London) **465**, 763 (2010).

[25] B. Fischer, M. Kremer, T. Pfeifer, B. Feuerstein, V. Sharma, U. Thumm, C. D. Schröter, R. Moshammer, and J. Ullrich, Phys. Rev. Lett. **105**, 223001 (2010).

[26] K. P. Singh, F. He, P. Ranitovic, W. Cao, S. De, D. Ray, S. Chen, U. Thumm, A. Becker, M. M. Murnane, H. C. Kapteyn, I. V. Litvinyuk, and C. L. Cocke, Phys. Rev. Lett. **104**, 023001 (2010).

[27] F. Anis and B. D. Esry, Phys. Rev. Lett. **109**, 133001 (2012).

[28] I. Znakovskaya, P. von den Hoff, G. Marcus, S. Zherebtsov, B. Bergues, X. Gu, Y. Deng, M. J. J. Vrakking, R. Kienberger, F. Krausz, R. de Vivie-Riedle, and M. F. Kling, Phys. Rev. Lett. **108**, 063002 (2012).

[29] A. González-Castrillo, A. Palacios, H. Bachau, and F. Martín, Phys. Rev. Lett. **108**, 063009 (2012).

[30] N. G. Kling, K. J. Betsch, M. Zohrabi, S. Zeng, F. Anis, U. Ablikim, B. Jochim, Z. Wang, M. Kübel, M. F. Kling, K. D. Carnes, B. D. Esry, and I. Ben-Itzhak, Phys. Rev. Lett. **111**, 163004 (2013).

[31] T. Rathje, A. M. Sayler, S. Zeng, P. Wustelt, H. Figger, B. D. Esry, and G. G. Paulus, Phys. Rev. Lett. **111**, 093002 (2013).

[32] X. C. Gong, P. L. He, Q. Y. Song, Q. Y. Ji, H. F. Pan, J. X. Ding, F. He, H. P. Zeng, and J. Wu, Phys. Rev. Lett. **113**, 203001 (2014).

[33] H. Xu, Z. C. Li, F. He, X. Wang, A. A. T. Noor, D. Kielpinski, R. T. Sang, and I. V. Litvinyuk, Nature Commun. **8**, 15849 (2017).

[34] Z. Chen, P. L. He, and F. He, Phys. Rev. A **101**, 033406 (2020).

[35] D. Yang and S.-L. Cong, Phys. Rev. A **84**, 013424 (2011).

[36] T. Fan *et al.*, Proc. Natl. Acad. Sci. USA **112**, 14206 (2015).

[37] P. Huang *et al.*, Nature Photonics **12**, 349 (2018).

[38] R. Kosloff and H. T. Ezer, Chem. Phys. Lett. **127**, 223 (1986).

[39] R. Kosloff and D. Kosloff, J. Comput. Phys. **52**, 35 (1983).

[40] F. He and U. Thumm, Phys. Rev. A **81**, 053413 (2010).

[41] J. M. Ngoko Djiokap, S. X. Hu, L. B. Madsen, N. L. Manakov, A. V. Meremianin, and A. F. Starace, Phys. Rev. Lett. **115**, 113004 (2015).

[42] J. M. Ngoko Djiokap, A. V. Meremianin, N. L. Manakov, S. X. Hu, L. B. Madsen, and A. F. Starace, Phys. Rev. A **94**, 013408 (2016).

[43] K. J. Yuan, S. Chelkowski, and A. D. Bandrauk, Phys. Rev. A **93**, 053425 (2016).

[44] D. Pengel, S. Kerbstadt, D. Johannmeyer, L. Englert, T. Bayer, and M. Wollenhaupt, Phys. Rev. Lett. **118**, 053003 (2017).

[45] D. Pengel, S. Kerbstadt, L. Englert, T. Bayer, and M. Wollenhaupt, Phys. Rev. A **96**, 043426 (2017).

[46] X. Xie, S. Roither, S. Larimian, S. Erattupuzha, L. Zhang, D. Kartashov, F. He, A. Baltuska, and M. Kitzler, Phys. Rev. A **99**, 043409 (2019).

[47] P. A. Orr, I. D. Williams, J. B. Greenwood, I. C. E. Turcu, W. A. Bryan, J. Pedregosa-Gutierrez, and C. W. Walter, Phys. Rev. Lett. **98**, 163001 (2007).

[48] J. McKenna, A. M. Sayler, F. Anis, B. Gaire, N. G. Johnson, E. Parke, J. J. Hua, H. Mashiko, C. M. Nakamura, E. Moon, Z. Chang, K. D. Carnes, B. D. Esry, and I. Ben-Itzhak, Phys. Rev. Lett. **100**, 133001 (2008).

[49] X. M. Tong and C. D. Lin, Phys. Rev. Lett. **98**, 123002 (2007).

[50] A. S. Alnaser, X. M. Tong, T. Osipov, S. Voss, C. M. Maharjan, B. Shan, Z. Chang, and C. L. Cocke, Phys. Rev. A **70**, 023413 (2004).